

Quantum Anomalous Layer Hall Effect in the Topological Magnet MnBi_2Te_4

Wen-Bo Dai,^{1,2} Hailong Li,¹ Dong-Hui Xu,³ Chui-Zhen Chen,^{4,5,*} and X. C. Xie^{1,6,7,2,†}

¹International Center for Quantum Materials, School of Physics, Peking University, Beijing 100871, China

²Beijing Academy of Quantum Information Sciences, Beijing 100193, China

³Department of Physics, Chongqing University, Chongqing 400044, China

⁴School of Physical Science and Technology, Soochow University, Suzhou 215006, China

⁵Institute for Advanced Study, Soochow University, Suzhou 215006, China

⁶Collaborative Innovation Center of Quantum Matter, Beijing 100871, China

⁷CAS Center for Excellence in Topological Quantum Computation,
University of Chinese Academy of Sciences, Beijing 100190, China

(Dated: June 27, 2022)

Recently, a type of Hall effect due to an unusual layer-locked Berry curvature called the layer Hall effect (LHE) has been reported in the even-layered two-dimensional antiferromagnetic (AFM) MnBi_2Te_4 [A. Gao *et.al*, *Nature* 595, 521 (2021)]. In this work, we report that the quantization of LHE, which we call the quantum anomalous layer Hall effect (QALHE), can be realized in MnBi_2Te_4 . The QALHE originates from kicking a layer-locked Berry-curvature monopole out of the Fermi sea by a vertical electric field. Remarkably, we demonstrate that the electric-field reversal can switch the sign of the quantized Hall conductance of QALHE in the even-layered AFM phase. The QALHE can also be realized in the ferromagnetic phase. These results provide a promising way toward the electric engineering of the Berry curvature monopoles and quantized-layered transport in topological magnets.

Introduction.—The quantum Hall effect observed in strong magnetic fields is one of most striking phenomena in condensed matter physics [1, 2]. Recently, the notion of the quantum Hall effect is generalized to quantum spin Hall effect [3–8] and quantum valley Hall effect [9, 10] by utilizing spin and valley degrees of freedom. They can be used to transport spin and valley current without dissipation, having potential applications in designing low-power devices. Yet, the electrons of opposite spin or valley indices in real materials spatially overlap with each other, leading to inevitable backscattering and thus short lifetimes of electron states [6, 8, 11], which hinders the development of these areas. Therefore, a new class of robust quantum Hall effect characterized by spatial-resolved topological index is highly desirable.

Recently, significant progresses have been achieved to realize layered topologically magnetic systems [12–18]. In particular, the intrinsic antiferromagnetic (AFM) topological insulator (TI) MnBi_2Te_4 has become a highly tunable platform to realize various of exotic topological phenomena due to the interplay between the Berry phase and its rich internal magnetic structures [19–25]. Notably, an intriguing Hall effect named the layer Hall effect (LHE) [26] has been identified in the even-layered AFM MnBi_2Te_4 . As shown in Fig. 1(a), the LHE manifests emerging layer-dependent Hall current flowing in different directions, because opposite Berry curvature is locked to top and bottom layers of MnBi_2Te_4 . If the net Berry curvature is generated under an electric field, a layer-polarized anomalous Hall effect (AHE) arises in the LHE system. This creates a new pathway to the spatial-tailoring of the Berry curvature via electric manipulation. It is natural to conceive of further generalizing the LHE to its quantized version.

In this work, we propose layer-polarized quantum anomalous Hall effect (QAHE) in the disordered topological magnet MnBi_2Te_4 under electric field, where a net Berry curvature monopole is locked to top or bottom layer [see Fig. 1(b)]. This can be regarded as a quantized version of the LHE, so we call it the quantum anomalous layer Hall effect (QALHE). Remarkably, in the even-layered AFM MnBi_2Te_4 , we demonstrate that the electric-field reversal can switch the sign of the quantized total Hall conductance, where the quantized layer-dependent Hall conductance is switched between top and bottom layers [see Fig. 1(c)]. That's because that an electric field along the z -axis can transfer a net layer-locked topological monopole to above the Fermi level on the top or bottom layer [Figs. 1(d) and (f)]. Here, the Berry-curvature monopole manifests as disorder-induced quantized Berry curvature in the energy space, which are locked to the layer index [Fig. 1(e)] and will shift in the energy space under electric fields. To capture the underlying physics, we investigate the evolution of the Berry curvature and the ratio of the geometric mean density of states (DOS) ρ_{typ} to the arithmetic mean DOS ρ_{avr} . In addition, we show that QALHE can also be realized in the ferromagnetic (FM) MnBi_2Te_4 . **Model Hamiltonian.**—The disordered MnBi_2Te_4 under E field can be described by a 4×4 effective Hamiltonian $H = H_N(\mathbf{k}) + g_z^\mu H_m(\mathbf{k}) + U(z)$ [23–25]. Here, the nonmagnetic part and the magnetic part $g_z^\mu H_m$ in momentum space are respectively given by

$$H_N = \mathcal{E}(\mathbf{k}) + \begin{pmatrix} m_0(\mathbf{k}) & A_z k_z & 0 & A k_- \\ A_z k_z & -m_0(\mathbf{k}) & A k_- & 0 \\ 0 & A k_+ & m_0(\mathbf{k}) & -A_z k_z \\ A k_+ & 0 & -A_z k_z & -m_0(\mathbf{k}) \end{pmatrix}$$

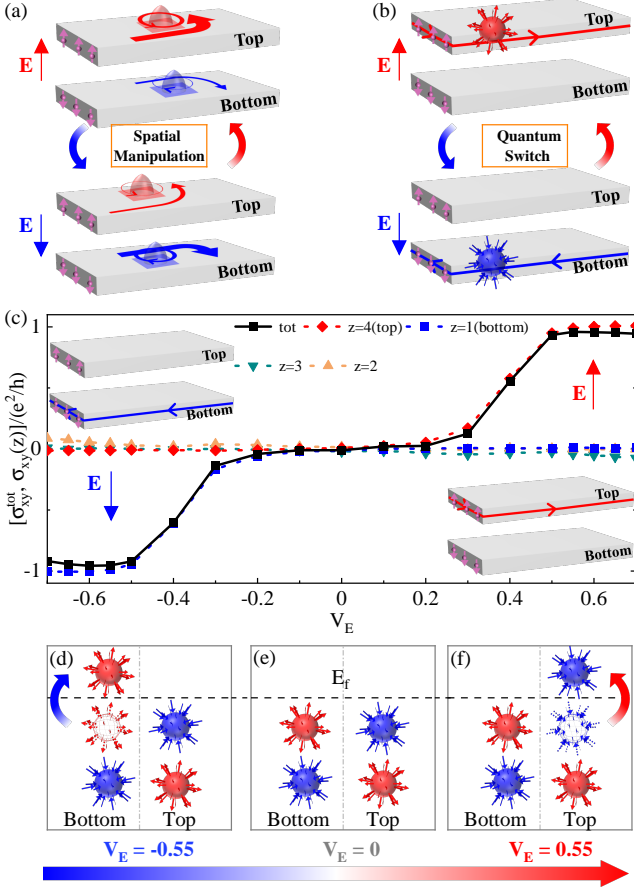


FIG. 1: (Color online). (a-b) Electric manipulation of the LHE and QALHE in even-layered AFM MnBi_2Te_4 . (a) Opposite Berry curvature locked to the top and bottom layers, which are depleted in different layers under vertical E field. Thus, the electrons deflecting in opposite directions cannot cancel, creating a net anomalous Hall current [26, 27]. (b) Quantum switch of the QALHE (quantization of the LHE) with opposite layer-locked Berry curvature monopoles, under vertical E field. (c) The Hall conductance of the whole system (solid line) σ_{xy}^{tot} and of each layer (dash lines) $\sigma_{xy}(z)$ versus the vertical E -field strength V_E in a four-layer AFM MnBi_2Te_4 . The Fermi energy is $E_f = 1.2$ and system size $N_x = N_y = 48$. The parameters are set as $g_z^- = (-1)^z$, $M_0 = -0.22$, $M_{1,2} = -0.22$, $A = 0.78$, $A_m = 0.44$, $A_z = 0.1$, $B_0 = 1.1$, $B_{1,2} = 0.92$, $B_0^z = 0.2$ [23, 24] and other parameters equal to zero unless specified. (d-f) Schematic plots of the layer-locked positive (red sphere) and negative (blue sphere) Berry curvature monopoles for different V_E . The empty spheres in (d) and (f) indicate E -field-triggered Berry curvature monopoles transition across the Fermi level E_f .

and

$$H_m = \begin{pmatrix} m_1(\mathbf{k}) & 0 & 0 & A_m k_- \\ 0 & m_2(\mathbf{k}) & -A_m k_- & 0 \\ 0 & -A_m k_+ & -m_1(\mathbf{k}) & 0 \\ A_m k_+ & 0 & 0 & -m_2(\mathbf{k}) \end{pmatrix}$$

where $g_z^+ = 1$ and $g_z^- = (-1)^z$ describe the FM and AFM order, respectively. Here, the wave vectors $k_{\pm} = k_x \pm ik_y$,

$\mathcal{E}(\mathbf{k}) = D_z k_z^2 + D(k_x^2 + k_y^2)$, $m_\nu(\mathbf{k}) = M_\nu + B_\nu^z k_z^2 + B_\nu(k_x^2 + k_y^2)$. $U(z) = V_E[-(N_z + 1)/2 + z]$ represents the z th-layer potential along z -axis. The magnetic disorder is included as $H_W(\mathbf{r}) = V(\mathbf{r})\sigma_z$, where the random potential $V(\mathbf{r}) \in [-W/2, W/2]$ and the disorder strength $W = 3.5$ unless specified. The Pauli matrix σ_z acts on the spin subspace.

E-field triggered Berry curvature monopoles and QALHE.—Due to the parity-time (\mathcal{PT}) symmetry, the total Hall current of the even-layered AFM MnBi_2Te_4 system vanishes without external fields [27]. However, unlike nonmagnetic topological systems, an electric field can induce net Berry curvature and Hall currents in the AFM TI by breaking the \mathcal{PT} symmetry. To investigate the E -field-induced Hall effect, we evaluate the total Hall conductance $\sigma_{xy}^{\text{tot}} = \sum_z \sigma_{xy}(z)$, where the layer-dependent Hall conductance in the z -th layer $\sigma_{xy}(z) = C_z e^2/h$ and the layer-dependent Chern number C_z is given by [28, 29]

$$C_z = 2\pi i \langle \text{Tr} \{ P_{E_f} [-i[\hat{x}, P_{E_f}], -i[\hat{y}, P_{E_f}]] \} \rangle_z \rangle_W, \quad (1)$$

with P_{E_f} being the projector onto the occupied states of H below the Fermi energy E_f . \hat{x} (\hat{y}) is coordinate operator, and $\langle \dots \rangle_W$ means averaging over different disorder configurations.

Figure 1(c) plots the Hall conductance versus the E -field strength V_E . Remarkably, it is found that the electric-field reversal can flip the Hall conductance σ_{xy}^{tot} plateaus of the QAHE (see the black line). This is closely analogous to the electric-field-reversible anomalous Hall effect experimentally observed in the LHE system [26, 27], so we call it QALHE. Further, we compare the total Hall conductance σ_{xy}^{tot} with the layer-dependent Hall conductance $\sigma_{xy}(z)$. For $V_E > 0$, the $\sigma_{xy}^{\text{tot}} = e^2/h$ plateau is attributed to the $\sigma_{xy}(z = 4)$ of the top layer (see the red line), while (for $V_E < 0$) the $\sigma_{xy}^{\text{tot}} = -e^2/h$ plateau comes from the $\sigma_{xy}(z = 1)$ of the bottom layer (see the blue line). This means that the increase in upward (+ z) and downward (- z) electric field can drive top and bottom layer from a topologically trivial phase into the QAHE phase of $\sigma_{xy}(z) = \pm e^2/h$, respectively. Since the Hall conductance arises from the total Berry curvature of all the occupied states, there exist Berry curvature monopoles under the Fermi level in the QALHE. To this end, we provide a phenomenological explanation by using Berry curvature monopoles. In Fig. 1(e), at the zero electric field ($V_E = 0$), there exist a pair of positive and negative Berry curvature monopoles and the \mathcal{PT} -symmetric partner on the top and bottom layers, respectively. Here two degenerate Berry curvature monopoles are of opposite values on the top and bottom layers due to the \mathcal{PT} symmetry. As shown in Fig. 1(f), the monopoles of the top layer are lifted up in the energy space due to the upward electric field ($V_E > 0$), and they are transferred to above the Fermi energy E_f when $V_E > 0.55$ leaving a net (+1) Berry curvature monopole in the top layer

and the whole system under E_f . This explains why the upward electric field can drive the top-layer Hall conductance from $\sigma_{xy}(z) = 0$ into $\sigma_{xy}(z) = 1$ phase. A similar process can give rise to a net (-1) Berry curvature monopole in the bottom layer and the whole system under a negative electric field [see Fig.1(d)].

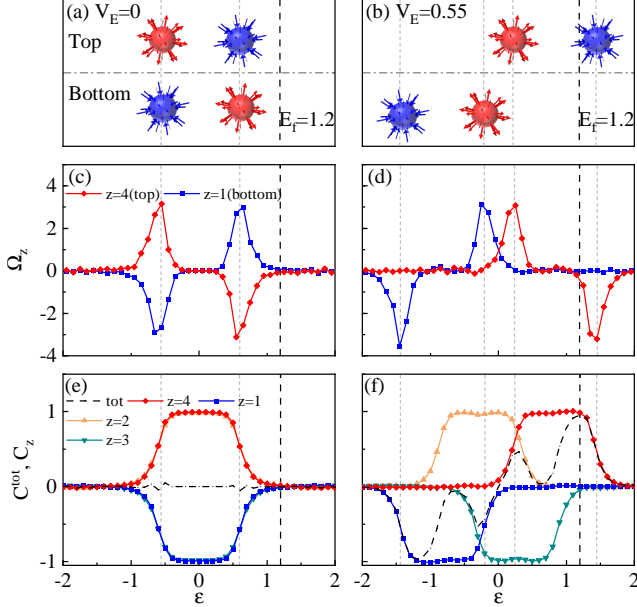


FIG. 2: (Color online). Evolutions of Berry-curvature monopoles in AFM MnBi_2Te_4 when the E field increases from (a) $V_E = 0$ to (b) $V_E = 0.55$. Corresponding, (c-d) the layer-dependent Berry curvature Ω_z vs the energy ε , and (e-f) the layer-dependent C_z and the total Chern numbers $C^{tot} = \sum_z C_z$. The Fermi energy $E_f = 1.2$ is fixed with the size $48 \times 48 \times 4$.

To quantitatively elucidate the evolution of the Berry curvature monopoles under the electric field, we calculated the layer-locked Berry curvature in energy space according to $C_z(\varepsilon) = \int_{-\infty}^{\varepsilon} \Omega_z(\epsilon) d\epsilon$ [30], where $\Omega_z(\varepsilon)$ is the Berry curvature of the z -th layer in energy space ε . Figure 2 plot the Berry curvature and Chern numbers, and sketch the corresponding Berry curvature monopole. In Fig.2(c) when $V_E = 0$, the top-layer-locked Berry curvature $\Omega_{z=4(top)}$ has two peaks for each layer, one positive and one negative, in the whole energy band. Each peak corresponds to a topological phase transition between $C_z = \pm 1$ to $C_z = 0$ at a critical energy ε_c [see Fig. 2(e)], which will become a delta function $\delta(\varepsilon - \varepsilon_c)$ in the thermodynamic limit. So each positive (negative) Berry curvature peak manifests as a Berry curvature monopole with charge $+1$ (-1) in energy space as shown in Fig. 2(a).

In Fig. 2(a), there exists one pair of Berry curvature monopoles for the top and bottom layers each below the Fermi energy $E_f = 1.2$, in accordance with those in Fig. 1(e). By increasing V_E to 0.55 in Fig.2 (b), the top layer-locked Berry curvature monopoles (peaks)

ascend to the $+\varepsilon$ direction, while the bottom layer-locked monopoles (peaks) descend to the $-\varepsilon$ direction in the energy space, due to the layer-dependent potential $U(z) = V_E[-(N_z + 1)/2 + z]$. When a negative monopole in the top layer moves across the Fermi surface [see the blue ball in Fig. 2(b)], the AFM system reaches a top-layer-polarized QAHE phase with $C^{tot} = C_{z=4(top)} = 1$ [see Fig. 2(f)], since there are only one positive monopole from the occupied states in the top layer and no net monopoles in the other layers. This explains the E -field-induced monopoles transition discussed in Fig.1(f). Similarly, an downward E field will transfer a positive monopole in the bottom layer to above the Fermi energy [see Fig.1(d)] due to the \mathcal{PT} symmetry [27].

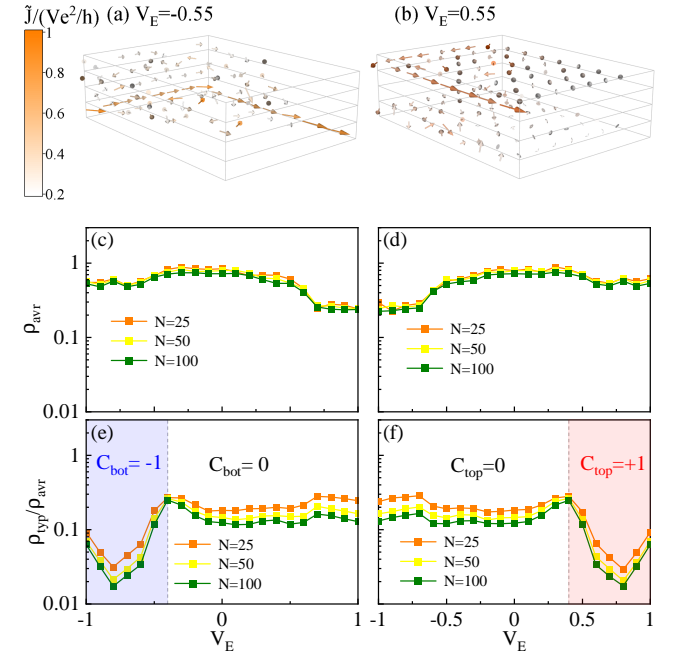


FIG. 3: (Color online). Local current of the QALH when the E -field is reversed from (a) $V_E = -0.55$ to (b) 0.55, with the system size $64 \times 64 \times 4$. (c-d) The arithmetic mean DOS ρ_{ave} , and (e-f) the ratio of the geometric mean DOS ρ_{typ} to ρ_{ave} for the bottom layer and the top layer, respectively. The different colored lines indicate different system sizes $N \times N \times 4$. Other parameters are the same as Fig. 2.

Quantum switch and scaling behavior.— The E -field switchable QALHE is accompanied by the switch of chiral edge channels on the boundary and layer-resolved topological phase transitions in the bulk [see Fig. 1(b)]. To verify this point, we first evaluate the local current using the recursive Green's function method [31], and then calculate the geometric mean DOS ρ_{typ} and the arithmetic mean DOS ρ_{ave} during the phase transition process. Here ρ_{typ} and ρ_{ave} are defined as [32–36]

$$\rho_{ave}(E_f) = \langle \langle \rho(i, E_f) \rangle \rangle \quad (2)$$

$$\rho_{typ}(E_f) = \exp[\langle \langle \ln \rho(i, E_f) \rangle \rangle]$$

where $\langle\langle\cdots\rangle\rangle$ denotes the arithmetic average over the sample sites and disorder realizations. The local DOS on the Fermi energy E_f is determined by $\rho(i, E_f) = \sum_{l,n,\alpha} |\langle il | n\alpha \rangle|^2 \delta(E_f - E_n)$ where i, l denotes the site index, orbital index and n is the eigenvalue index. To calculate ρ_{typ} and ρ_{ave} , we approximate $\delta(x) \approx \eta/[\pi(x^2 + \eta^2)]$ with $\eta = 10^{-4}$, and diagonalize the lattice Hamiltonian with periodic boundary conditions in x and y directions. For an extended state that uniformly distributes over the sample, ρ_{typ} is almost the same as ρ_{ave} . In contrast, for a localized state concentrated on certain sites, ρ_{typ} will be extremely small. The ratio ρ_{typ}/ρ_{ave} keeps finite for extended states, while ρ_{typ}/ρ_{ave} approaches zero for localized states, in the thermodynamic limit.

Figures 3 (a)-(b) show the local current of the QALHE at $E_f = 1.2$. When the E field is reversed from $V_E = -0.55$ to 0.55 , the chiral edge mode is switched from the bottom to top layer. The nonzero local current in the bulk indicates the existence of the disorder-induced localized states. Also, the finite scaling-independent ρ_{ave} in Figs. 3(c-d) and vanishing ρ_{typ}/ρ_{ave} with increasing the size N in Figs. 3(e-f) at $V_E = \pm 0.5$ verify the existence of localized states. Furthermore, in Fig. 3(f), there exists one fixed point for the top layer at $V_E^c \approx 0.4$ where ρ_{typ}/ρ_{ave} is independent of N . This is coincident with layer-resolved transition point from $C_{top} = 0$ to $C_{top} = 1$ of the top layer [see the red line] in Fig. 1(c), where the Berry curvature monopole is crossing the Fermi level Fig.1(f). Similarly, the fixed point of ρ_{typ}/ρ_{ave} for the bottom layer at $V_E^c \approx -0.4$ in Fig. 3(e) agrees with the transition of the bottom layer [see the blue line] in Fig. 1(c). Therefore, the quantum switch process of the QALHE is accompanied by switching the layer-polarized edge states on the boundary and the layer-dependent Anderson transitions in the bulk.

QALHE and quantum switch in FM phase.—Recently, the high Chern number QAHE was experimentally discovered in the FM MnBi_2Te_4 [37] and in the 2D-layered TI heterostructures [17, 18], which suggests a new platform to realize richer topological phenomena. As shown by Fig. 4(c), the layer-dependent Chern numbers (C_1, C_2, C_3) are tuned from $(1, 0, 0)$ to $(0, 1, 0)$ and then to $(0, 0, 1)$ by varying the energy $\varepsilon = E_f = -1.25$, to 0 and then to 1.25, where the edge channel is switched from the bottom to the middle and then to the top layer [see Figs. 4(a)-(c)]. That's because the layer-dependent Chern numbers changes values when the Fermi energy goes across the discrete locations of the Berry curvature monopoles Fig. 4(b), which are determined by the layer-dependent Berry curvature in Fig. 4(d). Furthermore, we plot ρ_{typ}/ρ_{ave} of the whole system versus energy in Fig. 4(e), and find that the locations of critical points and the Berry-curvature monopoles coincide. These results suggest that the Anderson localization plays an important role in the quantum switch process of the QALHE.

In reality, the QAHLE can be realized in the much

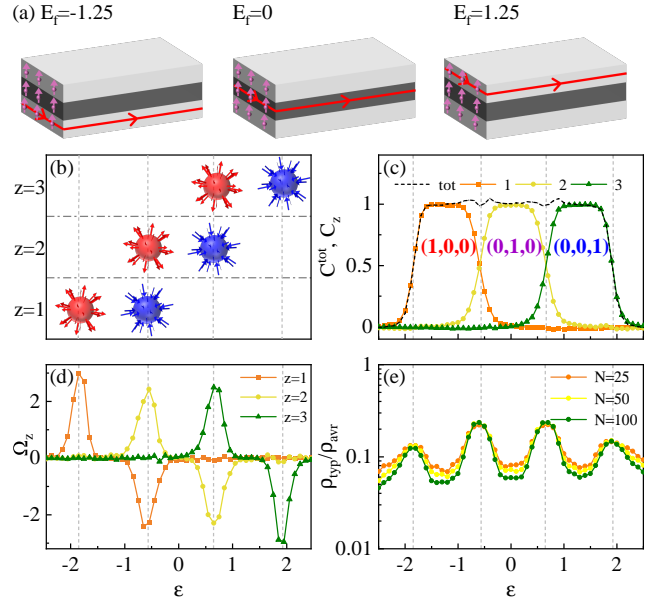


FIG. 4: (Color online). (a) Schematic plots of the QALHE in the FM MnBi_2Te_4 with the Fermi energies $E_f = -1.25, 0$ and 1.25 . (b) The layer-dependent Berry curvature monopoles, (c) The layer-dependent and total Chern numbers, and (d) the layer-dependent Berry curvature VS the energy ε . (e) The ratio of the geometric mean DOS to the arithmetic mean DOS ρ_{typ}/ρ_{ave} of the whole system for different system sizes $N \times N$. The dashed lines indicate that the locations of critical points in (e), and Berry curvature monopoles in (b) and (d) coincide. We set $g_z^+ = 1, M_0 = -0.3, M_{1,2} = -0.1, A = 0.78, A_m = 0.46, A_z = 0.1, B_0 = 1.1, B_{1,2} = 0.9, B_0^z = 0.2, D_z = 0.06$ [23]. The E field strength $V_E = 1.25$.

thicker FM topological magnet samples with higher Chern number (see the supplementary materials [27]) such as the FM MnBi_2Te_4 [37] and 2D-layered TI heterostructures [17]. Meanwhile, we propose that the quantum switch of the layer-dependent edge channel can be detected by a four-terminal device in experiments [27].

Discussions and conclusions.— The QAHLE can be viewed as a localization-driven counterpart to the recently reported LHE by A. Gao et al [26]. As a comparison, we have shown the LHE in the clean or weak disordered AFM MnBi_2Te_4 [27]. Moreover, the 3D AFM MnBi_2Te_4 is originally predicted to be an axion insulator exhibiting topological magnetoelectricity effect when the Fermi energy is inside the band gap [15, 16]. In contrast, to realize the QAHLE in the quasi-2D AFM MnBi_2Te_4 , the Fermi energy is tuned to the 2D Anderson-localized bulk states. In summary, we have revealed that the QALHE, a quantized version of the LHE, can be realized in both the AFM and FM MnBi_2Te_4 . The QALHE is attributed to electric-tunable the Berry-curvature monopoles. Further, we show that the electric field can switch the QALHE edge channel among different layers. Our work paves the way to electrically tunable layer-resolved dissipationless transport in topological

magnets.

Acknowledgement.— We thank Qing-Feng Sun for illuminating discussions. This work was financially supported by National Key R and D Program of China (Grant No. 2017YFA0303301), NBRPC (Grant No. 2015CB921102), NSFC (Grants Nos. 11534001, 11822407, 11921005, 12074108), and also supported by the Fundamental Research Funds for the Central Universities, the Strategic Priority Research Program of Chinese Academy of Sciences (DB28000000), and Beijing Municipal Science & Technology Commission (Grant No. Z191100007219013). C.-Z.C. is also funded by the Priority Academic Program Development of Jiangsu Higher Education Institutions.

* Electronic address: czchen@suda.edu.cn

† Electronic address: xcxie@pku.edu.cn

- [1] K. v. Klitzing, G. Dorda, and M. Pepper, *Phys. Rev. Lett.* **45**, 494 (1980).
- [2] D. J. Thouless, M. Kohmoto, M. P. Nightingale, and M. Den Nijs, *Phys. Rev. Lett.* **49**, 405 (1982).
- [3] C. L. Kane and E. J. Mele, *Phys. Rev. Lett.* **95**, 226801 (2005).
- [4] C. L. Kane and E. J. Mele, *Phys. Rev. Lett.* **95**, 146802 (2005).
- [5] B. A. Bernevig, T. L. Hughes, and S.-C. Zhang, *Science* **314**, 1757 (2006).
- [6] M. König, S. Wiedmann, C. Brune, A. Roth, H. Buhmann, L. W. Molenkamp, X.-L. Qi, and S.-C. Zhang, *Science* **318**, 766 (2007).
- [7] L. Du, I. Knez, G. Sullivan, and R.-R. Du, *Phys. Rev. Lett.* **114**, 096802 (2015).
- [8] S. Wu, V. Fatemi, Q. D. Gibson, K. Watanabe, T. Taniguchi, R. J. Cava, and P. Jarillo-Herrero, *Science* **359**, 76 (2018).
- [9] D. Xiao, W. Yao, and Q. Niu, *Phys. Rev. Lett.* **99**, 236809 (2007).
- [10] R. V. Gorbachev, J. C. W. Song, G. L. Yu, A. V. Kretinin, F. Withers, Y. Cao, A. Mishchenko, I. V. Grigorieva, K. S. Novoselov, L. S. Levitov, and A. K. Geim, *Science* **346**, 448 (2014).
- [11] K. Komatsu, Y. Morita, E. Watanabe, D. Tsuya, K. Watanabe, T. Taniguchi, and S. Moriyama, *Science Advances* **4** (2018), 10.1126/sciadv.aag0194.
- [12] Y. Gong, J. Guo, J. Li, K. Zhu, M. Liao, X. Liu, Q. Zhang, L. Gu, L. Tang, X. Feng, D. Zhang, W. Li, C. Song, L. Wang, P. Yu, X. Chen, Y. Wang, H. Yao, W. Duan, Y. Xu, S.-C. Zhang, X. Ma, Q.-K. Xue, and K. He, *Chinese Physics Letters* **36**, 076801 (2019).
- [13] E. D. L. Rienks, S. Wimmer, J. Sánchez-Barriga, O. Caha, P. S. Mandal, J. Růžicka, A. Ney, H. Steiner, V. V. Volobuev, H. Groiss, M. Albu, G. Kothleitner, J. Michalička, S. A. Khan, J. Minár, H. Ebert, G. Bauer, F. Freyse, A. Varykhalov, O. Rader, and G. Springholz, *Nature* **576**, 423 (2019).
- [14] M. M. Otrokov, I. I. Klimovskikh, H. Bentmann, D. Estyunin, A. Zeugner, Z. S. Aliev, S. Gaß, A. U. B. Wolter, A. V. Koroleva, A. M. Shikin, M. Blanco-Rey, M. Hoffmann, I. P. Rusinov, A. Y. Vyazovskaya, S. V. Ere-meev, Y. M. Koroteev, V. M. Kuznetsov, F. Freyse, J. Sánchez-Barriga, I. R. Amiraslanov, M. B. Babanly, N. T. Mamedov, N. A. Abdullayev, V. N. Zverev, A. Alfonsov, V. Kataev, B. Büchner, E. F. Schwier, S. Kumar, A. Kimura, L. Petaccia, G. D. Santo, R. C. Vidal, S. Schatz, K. Kißner, M. Ünzelmann, C. H. Min, S. Moser, T. R. F. Peixoto, F. Reinert, A. Ernst, P. M. Echenique, A. Isaeva, and E. V. Chulkov, *Nature* **576**, 416 (2019).
- [15] D. Zhang, M. Shi, T. Zhu, D. Xing, H. Zhang, and J. Wang, *Phys. Rev. Lett.* **122**, 206401 (2019).
- [16] J. Li, Y. Li, S. Du, Z. Wang, B.-L. Gu, S.-C. Zhang, K. He, W. Duan, and Y. Xu, *Science Advances* **5** (2019), 10.1126/sciadv.aaw5685.
- [17] Y.-F. Zhao, R. Zhang, R. Mei, L.-J. Zhou, H. Yi, Y.-Q. Zhang, J. Yu, R. Xiao, K. Wang, N. Samarth, M. H. W. Chan, C.-X. Liu, and C.-Z. Chang, *Nature* **588**, 419 (2020).
- [18] Y.-F. Zhao, R. Zhang, L.-J. Zhou, R. Mei, Z.-J. Yan, M. H. W. Chan, C.-X. Liu, and C.-Z. Chang, “Zero magnetic field plateau phase transition in higher chern number quantum anomalous hall insulators,” (2021).
- [19] Y. Deng, Y. Yu, M. Z. Shi, Z. Guo, Z. Xu, J. Wang, X. H. Chen, and Y. Zhang, *Science* **367**, 895 (2020).
- [20] J. Ge, Y. Liu, J. Li, H. Li, T. Luo, Y. Wu, Y. Xu, and J. Wang, *National Science Review* **7**, 1280 (2020).
- [21] C. Liu, Y. Wang, H. Li, Y. Wu, Y. Li, J. Li, K. He, Y. Xu, J. Zhang, and Y. Wang, *Nature Materials* **19**, 522 (2020).
- [22] R.-X. Zhang, F. Wu, and S. Das Sarma, *Phys. Rev. Lett.* **124**, 136407 (2020).
- [23] B. Lian, Z. Liu, Y. Zhang, and J. Wang, *Phys Rev Lett* **124**, 126402 (2020).
- [24] H. Sun, B. Xia, Z. Chen, Y. Zhang, P. Liu, Q. Yao, H. Tang, Y. Zhao, H. Xu, and Q. Liu, *Phys Rev Lett* **123**, 096401 (2019).
- [25] H. Li, H. Jiang, C. Z. Chen, and X. C. Xie, *Phys Rev Lett* **126**, 156601 (2021).
- [26] A. Gao, Y. F. Liu, C. Hu, J. X. Qiu, C. Tzschaschel, B. Ghosh, S. C. Ho, D. Berube, R. Chen, H. Sun, Z. Zhang, X. Y. Zhang, Y. X. Wang, N. Wang, Z. Huang, C. Felser, A. Agarwal, T. Ding, H. J. Tien, A. Akey, J. Gardener, B. Singh, K. Watanabe, T. Taniguchi, K. S. Burch, D. C. Bell, B. B. Zhou, W. Gao, H. Z. Lu, A. Bansil, H. Lin, T. R. Chang, L. Fu, Q. Ma, N. Ni, and S. Y. Xu, *Nature* **595**, 521 (2021).
- [27] See the supplementary materials for the layer Hall effect in the weak disorder strength, more discussions on the Berry curvature of the topological magnet MnBi_2Te_4 and the numerical methods. Additionally, the experimental characterization of the layer-locked QAHE edge mode.
- [28] E. Prodan, *Phys. Rev. B* **80**, 125327 (2009).
- [29] E. Prodan, *Journal of Physics A: Mathematical and Theoretical* **44**, 113001 (2011).
- [30] C.-Z. Chen, J. Qi, D.-H. Xu, and X. Xie, *Science China Physics, Mechanics & Astronomy* **64**, 1 (2021).
- [31] H. Jiang, L. Wang, Q.-f. Sun, and X. C. Xie, *Phys. Rev. B* **80**, 165316 (2009).
- [32] Y.-Y. Zhang, R.-L. Chu, F.-C. Zhang, and S.-Q. Shen, *Phys. Rev. B* **85**, 035107 (2012).
- [33] Y.-Y. Zhang and S.-Q. Shen, *Phys. Rev. B* **88**, 195145 (2013).
- [34] V. Dobrosavljević, A. A. Pastor, and B. K. Nikolić, *Eu-*

- rophysics Letters (EPL) **62**, 76 (2003).
- [35] G. Schubert, J. Schleede, K. Byczuk, H. Fehske, and D. Vollhardt, *Phys. Rev. B* **81**, 155106 (2010).
- [36] M. Janssen, *Physics Reports* **295**, 1 (1998).
- [37] J. Ge, Y. Liu, J. Li, H. Li, T. Luo, Y. Wu, Y. Xu, and J. Wang, *National Science Review* **7**, 1280 (2020).

Supplementary Materials for “Quantum Anomalous Layer Hall Effect in the Topological Magnet MnBi_2Te_4 ”

Wen-Bo Dai,^{1,2} Hailong Li,¹ Dong-Hui Xu,³ Chui-Zhen Chen,^{4,5,*} and X. C. Xie^{1,6,7,2,†}

¹International Center for Quantum Materials, School of Physics, Peking University, Beijing 100871, China

²Beijing Academy of Quantum Information Sciences, Beijing 100193, China

³Department of Physics, Chongqing University, Chongqing 400044, China*

⁴School of Physical Science and Technology, Soochow University, Suzhou 215006, China

⁵Institute for Advanced Study, Soochow University, Suzhou 215006, China

⁶Collaborative Innovation Center of Quantum Matter, Beijing 100871, China

⁷CAS Center for Excellence in Topological Quantum Computation, University of Chinese Academy of Sciences, Beijing 100190, China

(Dated: June 27, 2022)

S1. THE LAYER HALL EFFECT IN THE WEAK DISORDERED MnBi_2Te_4

In this section, we show that the layer Hall effect (LHE) exists in the even-layered antiferromagnetic (AFM) MnBi_2Te_4 in the clean limit or with the weak disorder strength. In Fig. S1(a), we plot the Hall conductance as a function of the electric-field strength V_E with $E_f = 1.2$. One can see that the anomalous Hall effect (AHE) with the positive or negative Hall conductance is induced by the top or bottom layer-polarized net Berry curvature under an upward or downward vertical electric field. Alternatively, in Fig. S1(b), we find that tuning the Fermi energy E_f can induce a transition from the top layer-polarized AHE with the positive net Berry curvature to the bottom layer-polarized AHE with negative net Berry curvature. Note that the LHE is sustainable to weak disorder at $W = 1$ (see the solid line in Fig. S1(a-b)). These results are qualitatively consistent with those discovered in the recent experiment.

The LHE can be understood by the band theory in the clean limit as follows. Generally, as shown in Fig. S1(c-d), there are one pair of conduction band with positive Berry curvature (red line) and valence band with negative Berry curvature (blue line) for the top layer, while the other pair of degenerate parity-time-reversal bands for the bottom layer are of opposite Berry curvature. To be specific, in Fig. S1(c), the bands of the top and the bottom layer are degenerate with the opposite Berry curvature in the absence of the electric field. Then, by applying an upward (downward) electric field, the band degeneracy is lifted, giving rise to a net positive (negative) Berry curvature or Hall conductance in the whole system [see Fig. S1(c)]. Similarly, in Fig. S1(d), when the system starts from a fixed upward electric field ($V_E = 1.2$), tuning the Fermi energy E_f across the neutral point ($E_f = 0$) can create a crossover from net negative bottom-layer-locked Berry curvature to net negative top-layer-locked Berry curvature.

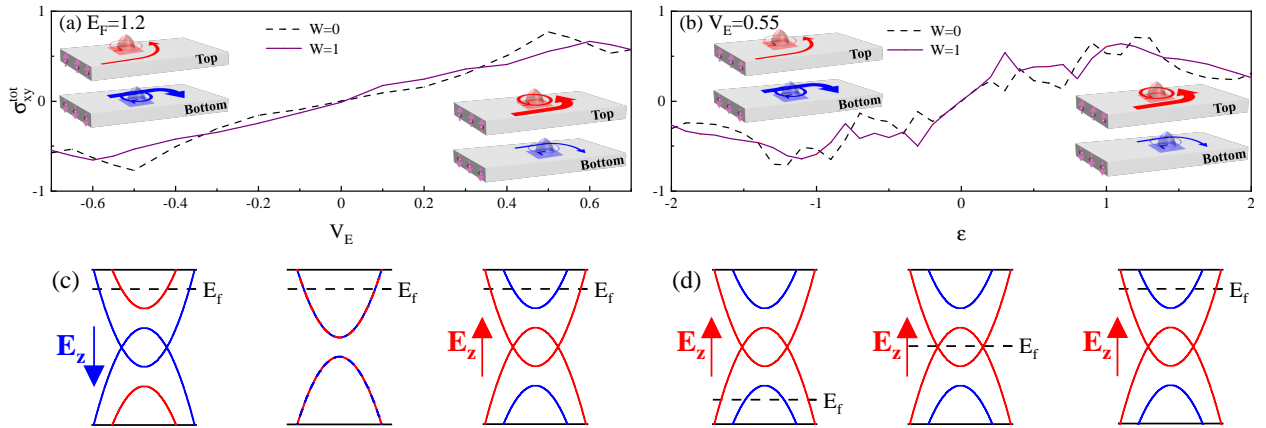


FIG. S1. (a) The total Chern number C_{tot} as a function of electric field V_E with Fermi energy $E_f = 1.2$. (b) The total Chern number C_{tot} as a function of electric field E_f with Fermi energy $V_E = 0.55$. (c)-(d) The schematic of the evolution of the energy band with varying V_E or E_f corresponding to (a)-(b)

* czchen@suda.edu.cn

† xcxie@pku.edu.cn

S2. \mathcal{PT} SYMMETRY AND THE LAYER-DEPENDENT BERRY CURVATURE

In Fig. 2 of the main text, we have quantitatively elucidated how an upward electric field creates a Berry-curvature monopole on the bottom layer. Due to the parity-time (\mathcal{PT}) symmetry, the upward electric field can drive a positive monopole in the top layer to above the Fermi energy. Here, we consider the situation with a downward electric field. In Fig. S2, we evaluate the Chern number and the Berry curvature as a function energy ϵ , and then schematically plot the Berry curvature monopoles correspondingly in the energy space. Comparing to the Fig. 2 of the main text, one can find that the downward electric field can trigger a positive monopole on the bottom layer to above the Fermi energy.

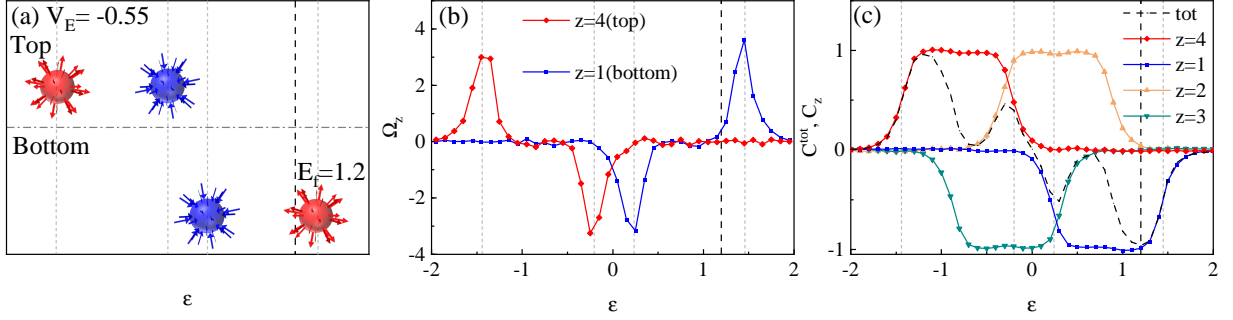


FIG. S2. (color online) (a) Schematic plots of the the Berry-curvature monopoles in AFM MnBi_2Te_4 when the E field strength $V_E = -0.55$. Corresponding, (b) shows layer-dependent Berry curvature versus the energy ϵ , and (c) shows the layer-dependent and the total Chern numbers. The Fermi energy $E_f = 1.2$ is fixed with the system size $48 \times 48 \times 4$.

Next, we will prove that, due to the \mathcal{PT} symmetry of the even-layered AFM MnBi_2Te_4 without external fields (see H in the main text), the reverse vertical electric field can polarize the Berry curvature of the opposite value on the opposite ($+z$ and $-z$) layers, i.e.

$$\begin{aligned} C_z(E_f, -V_E) &= -C_{\mathcal{P}z}(E_f, +V_E) \\ \Omega_z(\epsilon, -V_E) &= -\Omega_{\mathcal{P}z}(\epsilon, +V_E) \end{aligned} \quad (\text{S1})$$

For simplicity, we denote $\mathcal{PT} = \Theta$ and it is straight forward to verify that

$$H(-V_E) \cdot \Theta = \Theta \cdot H(V_E) \quad (\text{S2})$$

where V_E is the E -field strength. If $|\epsilon(V_E)\rangle$ is an eigenstate of $H^-(V_E)$ with energy ϵ , its space-time \mathcal{PT} partner $\Theta|\epsilon(V_E)\rangle$ is an eigenstate of $H^-(-V_E)$ with energy ϵ . Thus, we can conclude that

$$P_{E_f}(-V_E) = \Theta P_{E_f}(V_E) \Theta^\dagger \quad (\text{S3})$$

If we denote $[\hat{x}, P(V_E)] = K^{(x)}(V_E)$, the real-space noncommutative Kubo formula can be expressed as [1, 2]

$$\begin{aligned} C_z(E_f, V_E) &= \sigma_{xy}(z, E_f, V_E) / (e^2/h) \\ &= 2\pi i \cdot \text{Tr} \{ P_{E_f}(V_E) [-i[\hat{x}, P_{E_f}(V_E)], -i[\hat{y}, P_{E_f}(V_E)]] \}_z \\ &= -2\pi i \cdot \text{Tr} \{ P_{E_f}(V_E) [K_{E_f}^{(x)}(V_E), K_{E_f}^{(y)}(V_E)] \}_z \end{aligned} \quad (\text{S4})$$

We can express $K^{(x)}(-V_E)$ by using $P(-V_E)$ in Eq. S3 as

$$\begin{aligned}
K^{(x)}(-V_E) &= [\hat{x}, P(-V_E)] \\
&= i \sum_{m=1}^Q \{C_m(e^{-im\hat{x}\Delta_i} P(-V_E) e^{im\hat{x}\Delta_i} - e^{im\hat{x}\Delta_i} P(-V_E) e^{-im\hat{x}\Delta_i})\} \\
&= i \sum_{m=1}^Q \{C_m(e^{-im\hat{x}\Delta_i} \Theta P(V_E) \Theta^\dagger e^{im\hat{x}\Delta_i} - e^{im\hat{x}\Delta_i} \Theta P(V_E) \Theta^\dagger e^{-im\hat{x}\Delta_i})\} \\
&= \Theta \{-i \sum_{m=1}^Q \{C_m(e^{im\hat{x}\Delta_i} P(V_E) e^{-im\hat{x}\Delta_i} - e^{-im\hat{x}\Delta_i} P(V_E) e^{im\hat{x}\Delta_i})\}\} \Theta^\dagger \\
&= -\Theta K_{V_E}^{(-x)} \Theta^\dagger
\end{aligned} \tag{S5}$$

Replacing V_E with $-V_E$ and substituting Eq. S5 and Eq. S3 into Eq. S4 we have

$$\begin{aligned}
C_z(E_f, -V_E) &= -2\pi i \cdot \text{Tr}\{\Theta P_{E_f}(V_E) \Theta^\dagger [-\Theta K_{E_f}^{(-x)}(V_E) \Theta^\dagger, -\Theta K_{E_f}^{(-y)}(V_E) \Theta^\dagger]\}_z \\
&= -2\pi i \sum_{n \in z \& l, k \in \text{all}} \{P_{nl}^\Theta(V_E) (K_{l,k}^{(-x)\Theta}(V_E) K_{k,n}^{(-y)\Theta}(V_E) - K_{l,k}^{(-y)\Theta}(V_E) K_{k,n}^{(-x)\Theta}(V_E))\}
\end{aligned} \tag{S6}$$

where $O_{lk}^\Theta = \langle l | \Theta \hat{O} \Theta^\dagger | k \rangle$, n corresponds to the real space and orbital coordinates and l or k corresponds to an arbitrary basis. For an arbitrary operator \hat{O} , we can find

$$\begin{aligned}
O_{lk}^\Theta &= \langle l | \Theta \hat{O} \Theta^\dagger | k \rangle = \sum_{i,j} \{\langle l | \Theta O_{ij} | i \rangle \langle j | \Theta^\dagger | k \rangle\} \\
&= \sum_{i,j} \{O_{ij}^* \langle \Theta \Theta l | (-1) | \Theta i \rangle \langle \Theta j | (-1) | \Theta \Theta k \rangle\} \\
&= \sum_{i,j} \{O_{ij}^* \langle i | \Theta l \rangle \langle \Theta k | j \rangle\} = \sum_{i,j} \{\langle \Theta k | O_{ij}^* | j \rangle \langle i | \Theta l \rangle\} \\
&= \langle \Theta k | O^\dagger | \Theta l \rangle = O_{\Theta k, \Theta l}^\dagger
\end{aligned} \tag{S7}$$

Substituting it into Eq. S6, we have

$$\begin{aligned}
C_z(E_f, -V_E) &= -2\pi i \sum_{n \in z \& l, k \in \text{all}} \{P_{\Theta l, \Theta n}^\dagger(V_E) ((K^{(-x)\dagger}(V_E))_{\Theta k, \Theta l} (K^{(-y)\dagger}(V_E))_{\Theta n, \Theta k} \\
&\quad - (K^{(-y)\dagger}(V_E))_{\Theta k, \Theta l} (K^{(-x)\dagger}(V_E))_{\Theta n, \Theta k})\} \\
&= -2\pi i \sum_{n \in z} \{\langle \Theta n | [K_{E_f}^{(-y)}(V_E), K_{E_f}^{(-x)}(V_E)] P_{E_f}(V_E) | \Theta n \rangle\} \\
&= 2\pi i \cdot \text{Tr}\{P_{E_f}(V_E) [-i[-\hat{y}, P_{E_f}(V_E)], -i[-\hat{x}, P_{E_f}(V_E)]]\}_{\mathcal{P}z} \\
&= \sigma_{-y, -x}(z, E_f, V_E)/(e^2/h) = -\sigma_{xy}(z, E_f, V_E)/(e^2/h) \\
&= -C_{\mathcal{P}z}(E_f, V_E)
\end{aligned} \tag{S8}$$

Since $\Omega_z(\varepsilon) = d(C_z(\varepsilon))/d\varepsilon$, we can conclude Eq. S1 holds. Therefore, due to the \mathcal{PT} symmetry, reversing electric fields can trigger Berry- curvature monopoles with opposite value on the inverse layer.

Furthermore, if we take disorder into consideration, we will have $C_z(E_f, -V_E)[\omega] = C_z(E_f, -V_E)[\Theta\omega]$, where $\omega = \omega(\mathbf{r}, l)$ corresponds to one disorder configuration with a time-space \mathcal{PT} partner $\Theta\omega$. Here \mathbf{r}, l are the spatial and orbital indices. The even-layered AFM MnBi_2Te_4 with the disorder will recover the \mathcal{PT} symmetry after averaging over disorder configurations ω , because the probability of ω and $\Theta\omega$ equal with $\rho(\omega) = \rho(\Theta\omega)$. So, Eq. S1 also exists after averaging over disorder configurations ω .

S3. LOCAL CURRENT

In this section, we illustrate the details of how we evaluate the local current. We use a two-terminal device and apply a small voltage bias, $V_L - V_R$ between the left and right terminal of the device to simulate the local current

[3, 4]. By calculating the time derivative of the electron number and after some derivations, we can gain the currents between different sites

$$\begin{aligned}
J_i &= e \langle \dot{N}_i \rangle \\
&= \frac{ie}{\hbar} \left\langle \left[H, \sum_{\alpha} N_i \right] \right\rangle \\
&= \frac{2e}{\hbar} \sum_{\alpha, \beta, j} \int_{-\infty}^{eV_R} dE \operatorname{Im} \left\{ H_{i\alpha, j\beta} [G^r (\Gamma_L + \Gamma_R) G^a]_{j\beta, i\alpha} \right\} \\
&\quad + \frac{2e^2}{\hbar} \sum_{\alpha, \beta, j} \operatorname{Im} [H_{i\alpha, j\beta} G_{j\beta, i\alpha}^n(E_F)] (V_L - V_R) \\
&= \sum_{\alpha, \beta, j} J_{i \rightarrow j},
\end{aligned} \tag{S9}$$

where $J_{i \rightarrow j}$ is the current from the site \mathbf{i} to the site \mathbf{j} . $\Gamma_{L/R} = i [\Sigma_{L/R}^r - \Sigma_{L/R}^a]$ and $\Sigma_{L/R}^r (\Sigma_{L/R}^a)$ is the retarded (advanced) self energy. Besides $G^r (G^a)$ is the retarded (advanced) Green's function and $G_{j\beta, i\alpha}^n = (G^r \Gamma G^a)_{j\beta, i\alpha}$. Then the local current between $n_s \times n_s \times 1$ supercells $\tilde{J}_{i \rightarrow j}$ can be expressed as

$$\tilde{J}_{i \rightarrow j} = \sum_{\mathbf{m} \in \Omega_i} \sum_{\mathbf{n} \in \Omega_j} J_{\mathbf{m} \rightarrow \mathbf{n}}, \tag{S10}$$

where Ω_i (Ω_j) denotes the supercell with the coordinate \mathbf{i} (\mathbf{j}). If we only take the nearest-neighbor hopping into consideration, the current between the supercells can be expressed as

$$\tilde{J}_{i \rightarrow i + \mathbf{e}_l} = \sum_{n_1=0}^{n_s-1} \sum_{n_2=0}^{n_s-1} J_{[\mathbf{r}_i - \sum_{\mu} n_{\mu} (1 - \delta_{\mu, l}) \mathbf{e}_{\mu}] \rightarrow [\mathbf{r}_i + \mathbf{e}_l - \sum_{\mu} n_{\mu} (1 - \delta_{\mu, l}) \mathbf{e}_{\mu}]}, \tag{S11}$$

where $\mathbf{r}_i = [i_1 \cdot n_s, i_2 \cdot n_s, i_3]$. Next, let us evaluate the local current with varying the Fermi energy E_f in the FM MnBi_2Te_4 . In Fig. S3 with $E_f = -1.25$, there exists only one chiral edge mode in the 1st layer and the edge mode

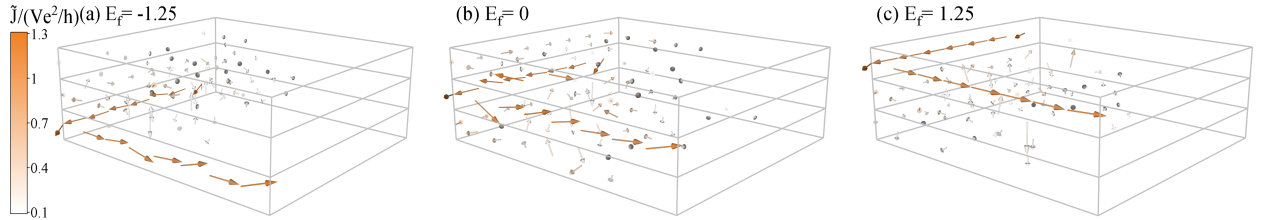


FIG. S3. (color online) (a) Local current of the QALH in the FM phase when the Fermi energy varying from (a) $E_f = -1.25$ to (b) 0 to (c) 1.25, with the E-field fixed $V_E = 1.2$ and system size $64 \times 64 \times 3$.

can be switched from the 1st layer to the 2nd layer and then to the 3rd layer by varying the energy $E_f = -1.25$ to 0 and then to 1.25, which is consistent with the schematic plots in Fig. 4(a) and numerical results in Fig. 4(c) in the main text. The local current in the bulk originates from the Anderson localized states induced by disorder.

S4. THE EXPERIMENTAL CHARACTERIZATION OF THE LAYER-LOCKED QAHE EDGE MODE

In this section, we will first show that the QALHE can also be realized in a much thicker system and we take the phase transitions $(1, 0, 0, \dots) \rightarrow (0, 1, 0, \dots) \rightarrow (0, 0, 1, \dots)$ in the FM MnBi_2Te_4 as an example. In Fig. S4(a-b), we plot the Chern numbers as a function of energy ϵ , and find that such phase transitions exist in four-layered and five-layered FM MnBi_2Te_4 by varying the energy ϵ , with the fixed electric field strength $V_E = 1.25$. Furthermore, we propose that the layer-locked QAHE edge mode can be detected by a four-terminal device as illustrated in Fig. S4(c1-c2). Here, leads 1 and 1' (2 and 2') are contacted to the left and right of the bottom (top) layer in order. According to the Landau-Buttiker formula, the transmission coefficient between leads i and j can be expressed as $T_{ij} = \text{Tr}\{\Gamma_i G^r \Gamma_j G^a\}$,

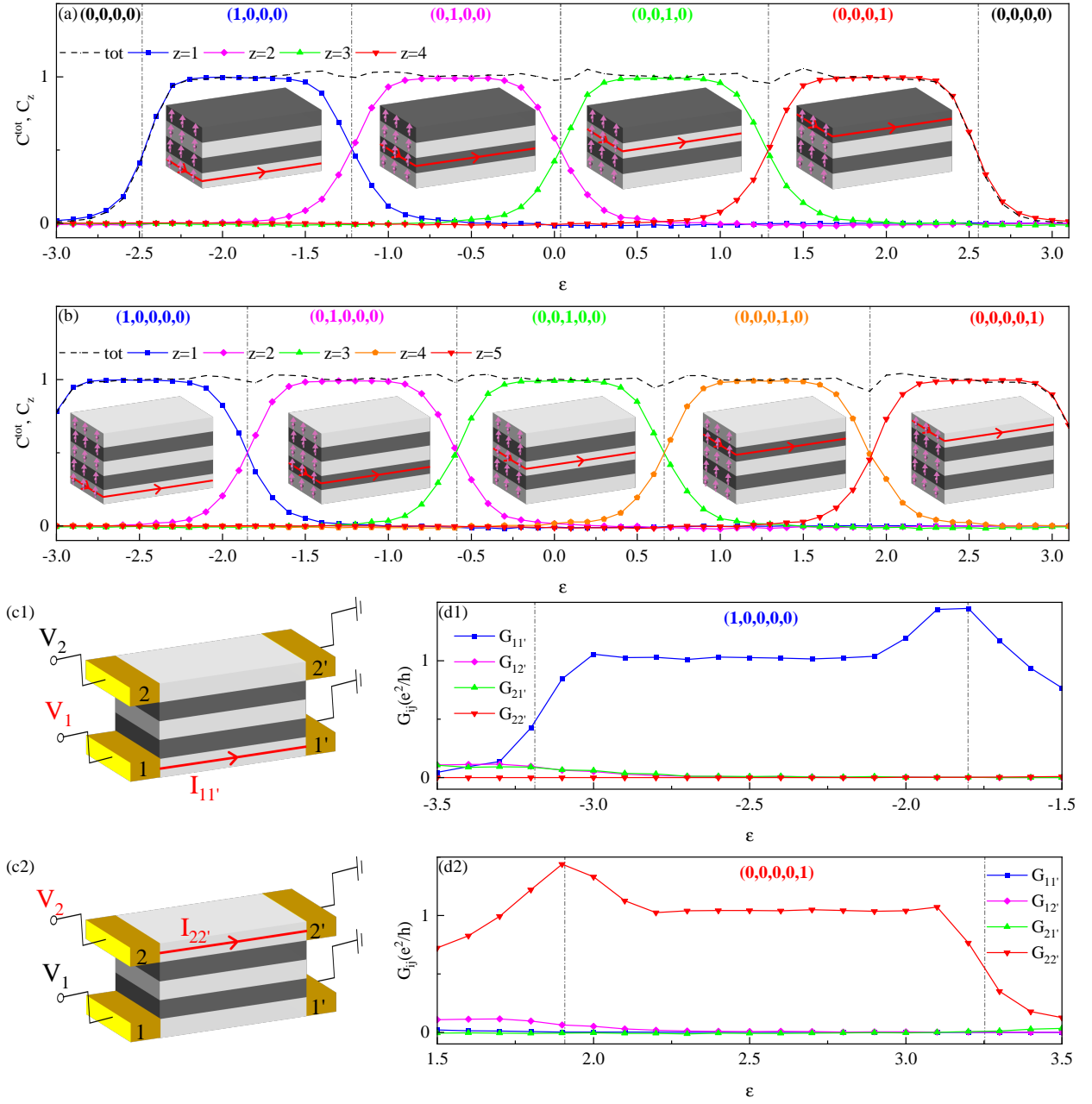


FIG. S4. (color online) (a)-(b) C^{tot}, C_z vs the Fermi energy E_f with E field fixed $V_E = 1.25$ in the four-layered or five-layered FM MnBi₂Te₄. (c1)-(c2) plot the schematic of the four-terminal device to detect the QALHE (d1)-(d2) plot G_{ij} when the bottom/top layer is polarized with the QAHE edge mode and correspond to (c1)-(c2).

where $G^{r,a}$ is retarded (advanced) Green's function of the whole system and Γ_i is the linewidth function of the i -th lead [5], and the related differential conductance is $G_{ij} = e^2/hT_{ij}$. When the five-layered FM is in the $(1,0,0,0,0)$ phase, a QAHE chiral edge mode exists only in the bottom layer. In this case, because the bottom layer is turned on and other layers is turned off, a current flows from lead 1 to lead 1' and current flow between other pair of leads, when the gate voltage $V_1(V_2)$ is applied on lead 1(lead 2) with other leads grounded. As a result, one can see $G_{11'} = e^2/h$ and the other conductances are zero([see Fig.S4(d1)]). On the other hand, in the $(0,0,0,0,1)$ phase, $G_{22'} = e^2/h$ and

the other conductances are zero since the chiral edge mode only exists in the top layer [see Fig. S4(d2)].

-
- [1] E. Prodan, *Phys. Rev. B* **80**, 125327 (2009).
 - [2] E. Prodan, *Journal of Physics A: Mathematical and Theoretical* **44**, 113001 (2011).
 - [3] H. Jiang, L. Wang, Q.-f. Sun, and X. C. Xie, *Phys. Rev. B* **80**, 165316 (2009).
 - [4] H. Li, H. Liu, H. Jiang, and X. C. Xie, *Phys. Rev. Lett.* **125**, 036602 (2020).
 - [5] S. Datta, *Electronic Transport in Mesoscopic Systems*, Cambridge Studies in Semiconductor Physics and Microelectronic Engineering (Cambridge University Press, 1995).